RSC Advances

PAPER

View Article Online
View Journal | View Issue

Cite this: *RSC Adv.*, 2022, **12**, 8559

High performance flame-retardant organic–inorganic hybrid epoxy composites with POSS and DOPO-based co-curing agent

Wei-Hua Xu, *[a] Shi-Jing Yan[a] and Jian-Qing Zhao*[b]

Received 28th December 2021
Accepted 8th March 2022

DOI: 10.1039/d1ra09401g

rsc.li/rsc-advances

Polyhedral oligomeric silsesquioxane (POSS) and a highly effective 9,10-dihydro-9-oxa-10-phosphaphenanthrene-10-oxide (DOPO)-based flame retardant co-curing agent (D-bp) were chemically introduced into the 4,4′-diaminodiphenyl methane (DDM)/diglycidyl ether of bisphenol A (DGEBA) epoxy system to create organic–inorganic hybrid epoxy composites with simultaneously improved flame retardancy and mechanical properties. The results revealed that POSS/D-bp/DGEBA hybrid composites exhibited excellent comprehensive performance, in which the V-0 criterion of the UL-94 test was passed and the peak of heat release rate (P-HRR) was significantly decreased from 939 to 371 kW m^{-2} when the phosphorus content was only 0.25 wt%. The glass transition temperature (T_g) increased by 16.2 °C and obvious improvement in the mechanical properties was also evidenced.

1. Introduction

Due to its characteristics of good chemical and corrosion resistance, high tensile strength and modulus, excellent dimensional stability and superior electrical properties, epoxy resin has been widely used as the polymeric matrix of advanced composites, especially in semiconductor encapsulation applications.[1–3] Unfortunately, flammability is one of the major disadvantages for epoxy resin, which limits the utilization in some fields that require high flame resistance.[4,5]

In recent years, as a substitute for halogen flame retardants, DOPO and its derivatives have exhibited remarkable achievements for halogen-free flame-retarded epoxy resin.[6–10] However, the weak bond of phosphorus-containing groups that introduced into the epoxy matrix reduces the crosslinking density and consequently brings negative effects on thermal and mechanical properties of cured epoxy resin.[11,12] It is still worthy to develop a high-performance epoxy resin which combines with the excellent flame retardancy, thermal and mechanical properties.

Organic–inorganic hybridization seems to be the effective way to realize such amelioration. POSS is considered to be an efficient inorganic reinforced material due to its well-defined nano-sized and typical cage structure. It has been widely used to improve the thermal and mechanical properties of thermoplastic or thermosetting polymers.[13,14] A representative POSS molecule structure with the general formula $(RSiO_{1.5})_n$ possesses a cube-octameric inorganic core which is constructed by Si–O–Si bond has excellent thermal properties.[15] Generally, R is a series of reactive groups (such as amino, epoxy, hydroxyl, *etc.*) which makes POSS possible to be chemically attached into the polymer matrix *via* copolymerization, grafting or blending.[16,17] Based on the above characteristics, POSS can optimize the matrix interactions by covalent bonding, and thereby improve the crosslinking density, which endows obvious exaltation to the polymer hybrid composites.[18–20] In addition, silicon and phosphorous element have exhibited the synergistic flame retardation effect through flame inhibition in the gas phase and char enhancement in the condensed phase.[21,22] Zhang and co-workers synthesized a novel flame retardant (DOPO–POSS) and proposed a flame retardant mechanism called "blowing-out extinguishing effect", which displayed excellent flame retardancy for epoxy resin through such synergism.[23–25] However, since DOPO–POSS was introduced *via* physical blending method, the flame retardant efficiency was limited and the mechanical properties of the modified thermoset would decreased seriously in contrary. Liu obtained POSS-bis-DOPO flame retardant from DOPO and amine POSS for epoxy resin. Unfortunately, the compatibility between POSS-bis-DOPO and epoxy matrix still needed to be further improved.[26] Hence, based on the synergism between phosphorus and silicon elements, in order to achieve a remarkable improvement in the flame-retardant efficiency by introducing silicon containing group into DOPO-based derivative and obtain excellent comprehensive properties, chemical approach such as copolymerization or grafting are considered as an effective method to realize phosphorus–silicon high efficiency synergistic flame retardant, which is the future development direction of high performance flame-retarded epoxy resin.

In our study, Glycidyl POSS (G-POSS) used as a reinforced matrix to substitute DGEBA and D-bp used as flame retardant

[a]*Key Laboratory of Chemistry and Engineering of Forest Products, State Ethnic Affairs Commission, School of Materials and Environment, Guangxi University for Nationalities, Nanning, Guangxi 530006, PR China. E-mail: xuweihua4848@163.com*
[b]*School of Materials Science and Engineering, South China University of Technology, Guangzhou, Guangdong 510640, PR China. E-mail: psjqzhao@scut.edu.cn*

co-curing of DDM thereby a series of POSS/D-bp/DGEBA hybrid composites were successfully prepared *via* organic–inorganic crosslinking reaction. The flame retardancy, thermal, mechanical and dynamic mechanical properties of cured hybrid composites were evaluated.

2. Experimental

2.1 Materials

DOPO and DGEBA (epoxide value of 0.51 mol per 100 g) were purchased from Eutec Trading (Shanghai) Co., Ltd and SINOPEC Assets Management Corporation Baling Petrochemical Branch, respectively. G-POSS (Fig. 1, epoxide value of 0.60 mol per 100 g), 4,4′-diaminodiphenyl methane (DDM) and 4-hydroxybenzaldehyde were obtained from Aladdin Chemistry (Shanghai) Co., Ltd. 1,4-Dioxane and ethanol were purchased from Guangzhou Chemical Reagent Factory and used without further purification. D-bp (Fig. 1, ^{1}H NMR (400 MHz, DMSO-d_6, ppm): 9.36–9.39 (s, 2H, Ph-OH), 8.15–8.17 (t, 2H, Ph-H), 7.96–7.99 (m, 2H, Ph-H), 7.72–7.74 (m, 2H, Ph-H), 7.66–7.70 (m, 2H, Ph-H), 7.51–7.53 (t, 2H, Ph-H), 7.38–7.44 (m, 2H, Ph-H), 7.28–7.32 (m, 2H, Ph-H), 7.18–7.19 (m, 2H, Ph-H), 7.13–7.15 (m, 2H, Ph-H), 7.01–7.03 (m, 2H, Ph-H), 6.68–6.70 (m, 2H, Ph-H), 6.64–6.66 (t, 2H, Ph-H), 6.61–6.63 (m, 2H, Ph-H), 6.52–6.55 (m, 2H, Ph-H), 6.47–6.50 (m, 2H, Ph-H), 6.43–6.45 (m, 2H, Ph-H), 6.38–6.42 (t, 1H), 5.97–6.01 (t, 1H), 4.83–4.88 (m, 1H, N–H), 3.39–3.44 (t, 2H). ^{31}P NMR (162 MHz, DMSO-d_6, ppm): 31.4, 28.6) was synthesized in our laboratory.[27]

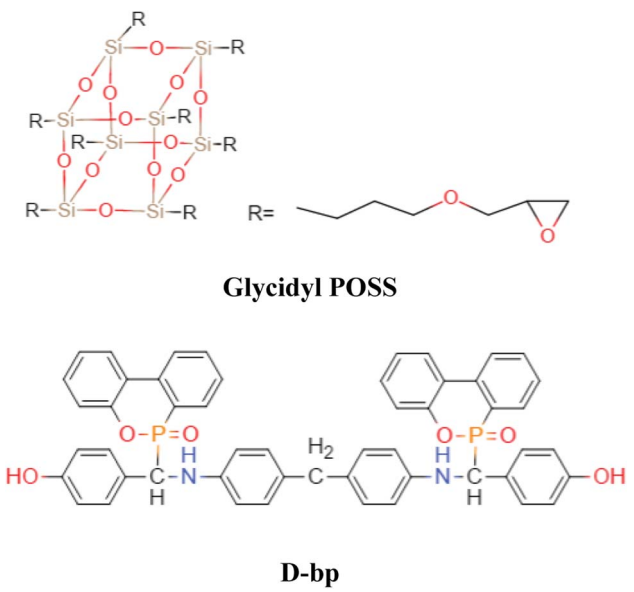

Fig. 1 Molecular structures of Glycidyl POSS and D-bp.

2.2 Preparation of POSS/D-bp/DGEBA hybrid composites

The stoichiometric formulations for POSS/D-bp/DGEBA hybrid composites are listed in Table 1, where the sum amount of amino and phenol groups from DDM and D-bp is equal to the epoxy groups from DGEBA and G-POSS. POSS/D-bp/DGEBA hybrid composites were prepared with the following thermal curing process. Firstly, DGEBA and D-bp were mixed at 140 °C by mechanical stirring under N_2 for 10 min. Then, the homogeneous liquid was cooled down to 90 °C and blended with G-POSS under ultrasonic dispersion for 1 h. After becoming transparent, DDM was added into the mixture and stirred until dissolved completely. Finally, all samples were vacuum-degassed in a mold and sequentially cured for 1 h at 80 °C, 1 h at 100 °C, 1 h at 120 °C, 3 h at 150 °C and 2 h at 180 °C, respectively.

2.3 Measurements

^{1}H and ^{31}P NMR spectra of D-bp were recorded on a Bruker AVANCE III HD 600 NMR instrument, and DMSO-d_6 was used as the solvent.

TGA was carried out on a Netzsch STA449F3 thermogravimetric analyzer with the temperature range from 30 °C to 800 °C at a heating rate of 10 °C min^{-1} under nitrogen and air atmosphere.

Flexural and tensile properties were studied in accordance with ASTM D638-08 and D790-07e using a Z010 universal testing machine. Samples were tested at a crosshead speed of 5 mm min^{-1} and the average value was adopted for each set of six specimens. Dynamic mechanical analysis (DMA) was conducted on a Netzsch DMA242C analyzer from 30 °C to 225 °C at a heating rate of 3 °C min^{-1} and a frequency of 10 Hz with three-point bending mode.

LOI measurement was conducted on an Fire Testing Technology FTA-SC48 oxygen index instrument with the sheet dimension of 150 × 6.5 × 3.2 mm^3 according to ASTM D2863-97. Vertical burning test was carried out on a Fire Testing Technology UL94-SC50 UL-94 flammability meter with the sheet dimension of 130 × 13 × 3.2 mm^3 according to ANSL UL 94-1985. Cone calorimeter test was carried out on a Fire Testing Technology FTT0007 cone calorimeter with the sheet

Table 1 Formulations of POSS/D-bp/DGEBA hybrid composites

Samples	DGEBA (g)	G-POSS (g)	DDM (g)	D-bp (g)	P (wt%)	Si (wt%)
EP-1	100	0	25.3	0	0	0
EP-2	95	5	25.5	0	0	0.68
EP-3	100	0	24.3	4.4	0.25	0
EP-4	95	5	24.5	4.4	0.25	0.66
EP-5	100	0	23.5	8.9	0.50	0
EP-6	95	5	23.8	8.9	0.50	0.64

dimension of 100 × 100 × 5 mm^3 according to ISO5660 under an external heat flux of 50 kW m^{-2}.

The char residues after cone calorimetry test were collected to investigate the condensed phase of hybrid composites. X-ray photoelectron spectroscopy (XPS) was carried out on a Kratos Axis Ultra-DLD X-ray photoelectron spectrometer with Al Kα radiation of 1486.6 eV.

The morphology of char residues after cone calorimeter test were observed by a FEI-NOVA NANOSEM 230 (EDS X-MAX50) scanning electron microscope (SEM) with an accelerating potential of 15 kV. The elemental analysis was conducted by the energy dispersive X-ray spectrometer (EDX) in the surface scanning model. The surface of char residues was sprayed with platinum before test.

3. Results and discussion

3.1 Flame retardancy of POSS/D-bp/DGEBA hybrid composites

3.1.1 UL-94 and LOI analysis. The results of UL-94 and LOI tests are presented in Table 2. It can be observed that no improvement in the UL-94 grade is obtained when G-POSS is solely incorporated into the DDM/DGEBA system for the silicon content of 0.68 wt%. The total combustion time (t_1 + t_2) decreases from lasting burning to 61.9 ± 3.1 seconds and the dripping phenomenon is disappeared, which indicating that the flame retardancy effect of G-POSS is limited. EP-5, which is only modified by D-bp with the phosphorus content of 0.50 wt%, exhibits a remarkable reduction in t_1 + t_2 and successfully attains V-0 rating in UL-94 classification with the LOI value of 39.7 ± 0.8% signifying the ameliorated flame retardancy of D-bp in DDM/DGEBA system. It is noteworthy that the concomitance of G-POSS and D-bp demonstrates exceptional result, in which the V-0 rating of UL-94 test is passed merely with the phosphorus content of 0.25 wt%. Besides, in the condition of same phosphorus content, POSS/D-bp/DGEBA hybrid composites exhibit a shorter t_1 + t_2 compare with the samples which only modified by D-bp. The above result illustrated that the flame retardant efficiency of D-bp is further enhanced by G-POSS which is attributed to the synergistic flame retardation effect between phosphorus and silicon elements.

Table 2 UL-94 and LOI tests results of POSS/D-bp/DGEBA hybrid composites[a,b]

		UL-94		
Samples	LOI (%)	t_1 + t_2 (s)	Dripping	Rating
EP-1	24.2 ± 0.9	Lasting burning	Yes	No rating
EP-2	25.5 ± 1.2	61.9 ± 3.1	No	No rating
EP-3	30.5 ± 1.4	14.5 ± 3.1	No	V-1
EP-4	30.7 ± 0.8	8.6 ± 1.1	No	V-0
EP-5	39.7 ± 0.8	6.7 ± 1.7	No	V-0
EP-6	39.6 ± 1.1	5.1 ± 1.4	No	V-0

[a] t_1: total combustion time after the first 10 s ignition. [b] t_2: total combustion time after the second 10 s ignition.

3.1.2 Cone calorimeter analysis. Cone calorimeter is an effective measurement to investigate the fire behavior of flame-retarded materials during the combustion. The collected combustion parameters, including time to ignition (TTI), the peak of heat release rate (P-HRR), total heat release (THR), the peak of smoke produce rate (P-SPR) and the average effective heat of combustion (av-EHC) are listed in Table 3 while the heat release rate (HRR), THR and smoke produce rate (SPR) curves are shown from Fig. 2–4, respectively. After D-bp is solely introduced into the DDM/DGEBA system, TTI has a downward trend. However, in the situation of same phosphorus content, POSS/D-bp/DGEBA hybrid composites display a longer TTI. It can be clearly observed from Fig. 2 that the HRR curve of EP-1 rapidly forms a sharp peak with the P-HRR value of 939 kW m^{-2}. The P-HRR value of EP-2 and EP-3 which respectively loading 0.68 wt% content of silicon and 0.25 wt% content of phosphorus firstly reduces to 753 and 767 kW m^{-2} with the incorporation of G-POSS or D-bp individually. Accompany with further introduction of D-bp, the P-HRR value obviously decreased to 651 kW m^{-2} and the time needed for reaching the peak value is lagged obviously. It is worth mentioning that the P-HRR value of POSS/D-bp/DGEBA hybrid composites, as shown in EP-4 and EP-6, decreases remarkably to 371 and 361 kW m^{-2} comparatively by 60.5% and 61.6% from EP-1 with the concomitance of G-POSS and D-bp. Meanwhile, it also can be observed in combination with Fig. 3 and 4 that THR and P-SPR of POSS/D-bp/DGEBA hybrid composites decrease significantly. THR and P-SPR

Table 3 Cone calorimetry results of POSS/D-bp/DGEBA hybrid composites[a,b,c,d]

Samples	TTI (s)	P-HRR (kW m^{-2})	THR (MJ m^{-2})	av-EHC (MJ kg^{-1})	P-SPR (m^2 s^{-1})	Residues (wt%)
EP-1	53	939	202	31.6	0.35	13.5
EP-2	48	753	175	29.2	0.33	17.1
EP-3	53	767	134	29.0	0.30	17.3
EP-4	54	371	116	23.9	0.22	25.9
EP-5	49	651	130	23.6	0.29	18.1
EP-6	51	361	115	21.3	0.20	28.5

[a] P-HRR: under the preset incident heat flux intensity, the maximum value of heat release rate per unit area after the material is ignited. [b] THR: the sum of the heat released by the material from ignition to flame extinction under the preset incident heat flow intensity. [c] EHC: the ratio of measured heat release rate to mass loss rate at a certain time reflects the combustion degree of volatile gas in gas phase flame. [d] P-SPR: the maximum value of specific extinction area (SEA) to mass loss rate (MLR).

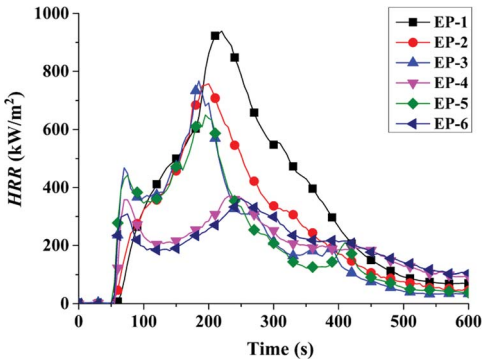

Fig. 2 HRR curve of POSS/D-bp/DGEBA hybrid composites.

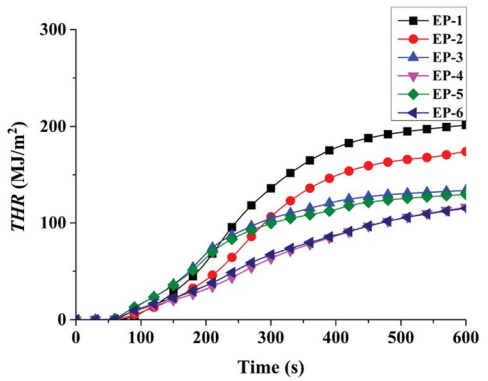

Fig. 3 THR curve of POSS/D-bp/DGEBA hybrid composites.

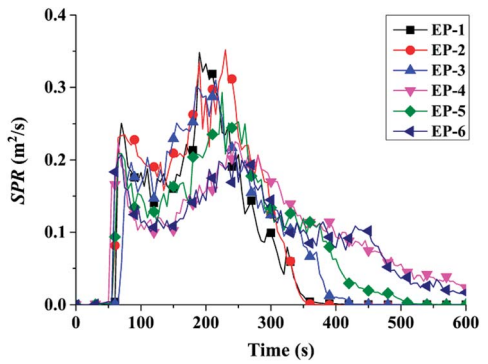

Fig. 4 SPR curve of POSS/D-bp/DGEBA hybrid composites.

values of EP-4 which achieved V-0 rating of UL-94 test have obviously decrease from 202 MJ m^{-2} and 0.35 m^2 s^{-1} of EP-1 to 116 MJ m^{-2} and 0.22 m^2 s^{-1} respectively when the sample only loading 0.25 wt% content of phosphorus. Besides, EP-6 has the lower THR and P-SPR values in the situation of same phosphorus content. What's more, contact the data in Table 3, the gradual decrement of EHC and significant increase in residues are revealed that the heat released by combustion in the condensed phase is obviously restrained. The above phenomena indicated that G-POSS and D-bp may have efficient synergistic flame retardation effects which play an important role for the enhancement of flame retardancy. The result of cone calorimetry test is consistent with the UL-94 and LOI tests.

3.2 TGA of POSS/D-bp/DGEBA hybrid composites

Fig. 5 shows the TG and DTG curves of POSS/D-bp/DGEBA hybrid composites under nitrogen and air atmospheres, respectively. The related decomposition data, including the initial decomposition temperature, which is defined as the temperature at 5% weight loss ($T_{d5\%}$), the temperature at maximum decomposition rate (T_{dmax}) and the residual mass at 800 °C (R_{800}) are summarized in Table 4, respectively. It can be observed from the TG curves of POSS/D-bp/DGEBA hybrid composites under nitrogen atmosphere that the thermal degradation process of all samples exhibits only one stage. Compared with EP-1, $T_{d5\%}$ and T_{dmax} values of EP-3 and EP-5 decrease concurrently following the introduction of flame retardant D-bp. The reasonable explanation is attributed to the fact that the bond energy of O=P–O is less than that of C–C bond so that the phosphorus-containing group first decomposes and generates phosphate or polyphosphate in a lower temperature. Nonetheless, $T_{d5\%}$ are still maintained in the high range of above 330 °C. On the contrary, for the same content of phosphorus, incorporation of G-POSS brings about an improvement in the $T_{d5\%}$ and T_{dmax} values, as shown from EP-4 and EP-6 whose $T_{d5\%}$ are 4.8 °C and 10.6 °C respectively higher than that of EP-3 and EP-5, and the same situation also appears on the T_{dmax} values which attributed to G-POSS possesses excellent thermal stability. Furthermore, the R_{800} values of POSS/D-bp/DGEBA hybrid composites are significantly increased following the flame retardation, with EP-6 exhibits the highest value of 25.6 wt%.

Under air atmosphere, the TG curves of POSS/D-bp/DGEBA hybrid composites exhibit two stages decomposition. The first stage attributes to the degradation of epoxy chains, and the second one corresponds to the decomposition between char residue and oxygen.[28,29] Compared with the unmodified EP-1, $T_{d5\%}$ and T_{dmax} values of EP-4 and EP-6 are reduced slightly, which means POSS/D-bp/DGEBA hybrid composites maintain good thermal stability in the air atmosphere. Additionally, combine with the DTG curves under nitrogen and air atmospheres that the mass loss rate of POSS/D-bp/DGEBA hybrid composites also significantly inhibited. The above results indicate the early degradation of phosphorus-containing group catalyzes the formation of carbon layer and G-POSS tends to stabilize the layer, which combine an effective barrier layer and improve the thermal properties and flame retardancy of POSS/D-bp/DGEBA hybrid composites.

3.3 Analysis of char residues of POSS/D-bp/DGEBA hybrid composites

3.3.1 Visual observation. The digital photographs of char residues after cone calorimetry test provide some useful information regarding the carbon layer structure. Fig. 6 intuitively displays that EP-1 combusted severely with less residue is traced. The utilization of G-POSS or D-bp individually, as shown in EP-2 and EP-3 significantly enhances the char residue and

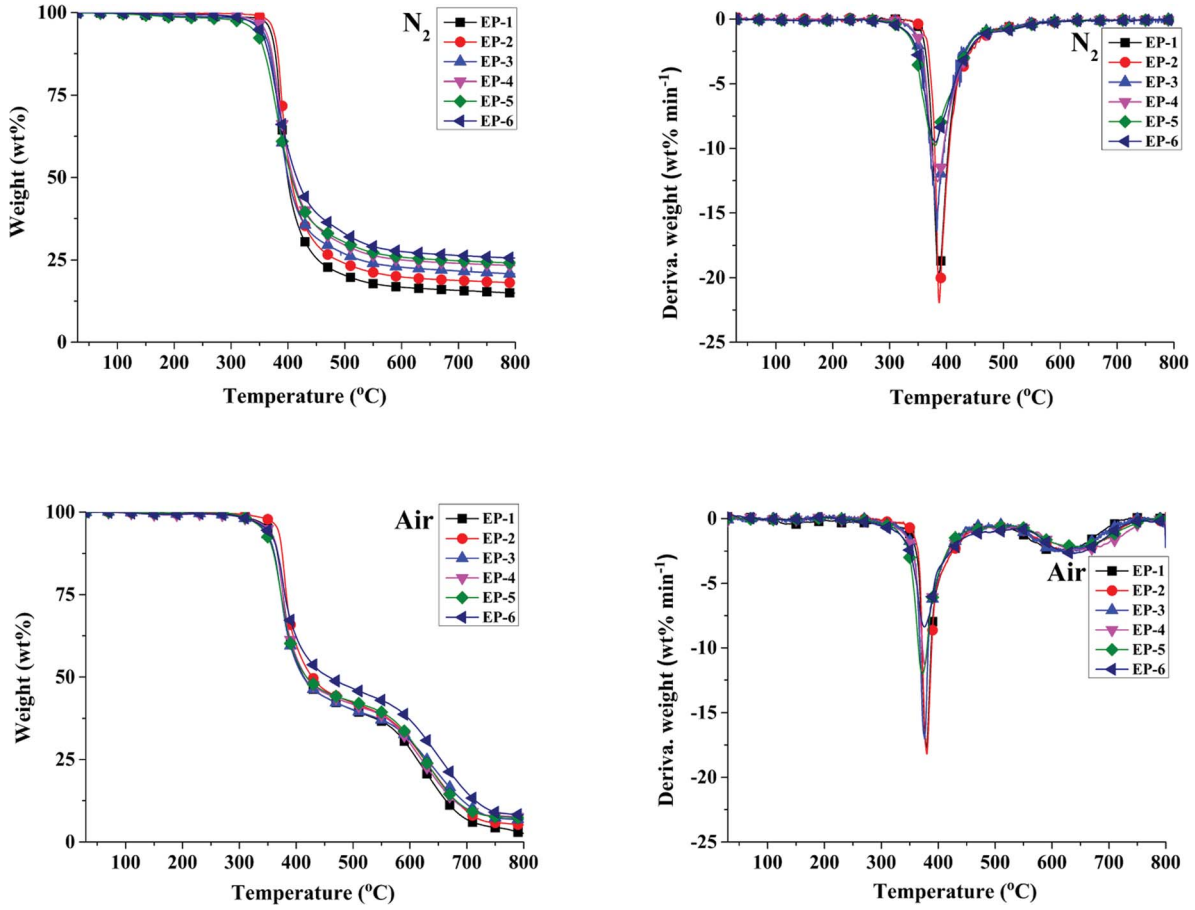

Fig. 5 TG and DTG curves of POSS/D-bp/DGEBA hybrid composites under nitrogen or air atmospheres.

Table 4 Thermal properties data of POSS/D-bp/DGEBA hybrid composites from TG and DTG curves

	Nitrogen			Air		
Samples	$T_{d5\%}$ (°C)	T_{dmax} (°C)	R_{800} (wt%)	$T_{d5\%}$ (°C)	T_{dmax} (°C)	R_{800} (wt%)
EP-1	368.0	386.6	14.9	351.1	378.9	2.6
EP-2	373.6	387.0	18.1	367.1	379.7	5.1
EP-3	353.6	382.9	20.8	342.3	376.3	6.8
EP-4	358.4	384.5	23.3	349.6	376.5	7.5
EP-5	338.4	379.9	24.1	340.1	372.1	7.2
EP-6	349.0	380.4	25.6	346.8	375.8	8.2

converts it to a dense honeycomb-like structure. Moreover, the char residues further turn into a more compact morphology in EP-4 and EP-6. Especially, the surface of EP-6 is obviously covered with white granulated substance, which may be attributed to the silicon dioxide (SiO_2) derived from the degradation of G-POSS. The visual observation of the char residue confirms the TGA results, in which the introduction of G-POSS and D-bp promotes the formation of relatively stable carbon layer which is able to inhibit the heat transfer more effectively during combustion.

3.3.2 SEM and EDX analysis. The exterior part of the char residues of POSS/D-bp/DGEBA hybrid composites after cone calorimeter test are collected and investigated by SEM (Fig. 7) and EDX element mapping (Fig. 8). From the Fig. 7 we can clearly observe that EP-1 exhibits a fragmented carbon layer and the debris seems loose while EP-2 presents numerous open porous holes that verify the failure of the layer to prevent the heat transfer. In contrast, EP-3 displays a thick and compact char layer structure and this outcome is seen more obviously in EP-4 and EP-6. In the EDX elements mapping image, we also can observed that the phosphorus element (P, in yellow) of EP-3 and EP-5 evenly distributed in the char residues. It is worth noting that EP-4 and EP-6 with the silicon element signal (Si, in blue) disperse very well in the P element, which indicates that the

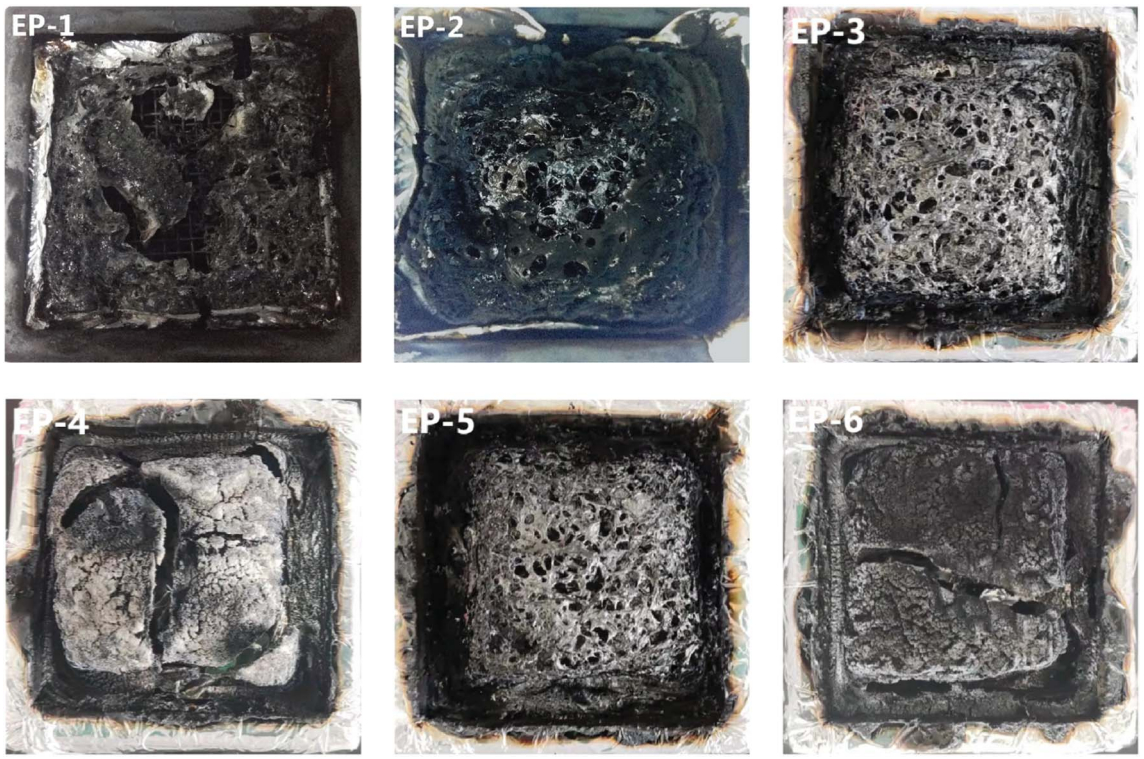

Fig. 6 Photographs of char residues from POSS/D-bp/DGEBA hybrid composites after cone calorimeter test.

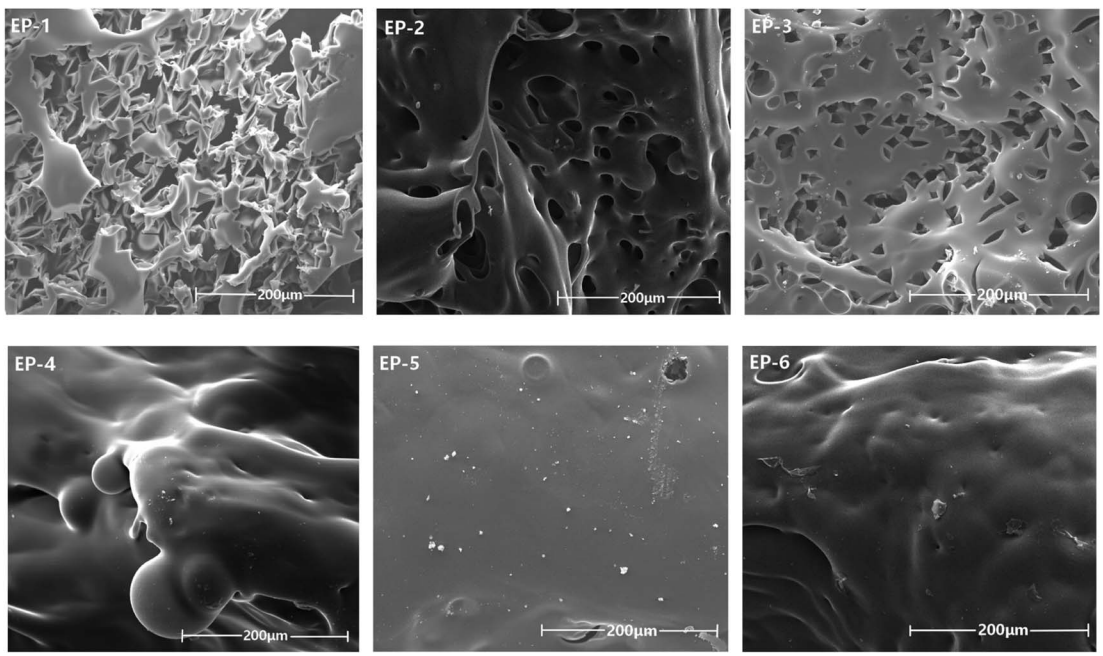

Fig. 7 SEM photographs of POSS/D-bp/DGEBA hybrid composites after cone calorimeter test (scale bar size: 200 μm).

stable and uniform carbon layer structure formed by phosphorus containing groups degraded from D-bp and silicon containing groups degraded from G-POSS can effectively prevent flame and heat transfer. The SEM and EDX results correspond well with the visual observation and cone calorimetric test results.

3.3.3 FT-IR analysis. Fig. 9 shows the FT-IR spectra of the exterior part of the char residues from EP-1, EP-3 and EP-6 after

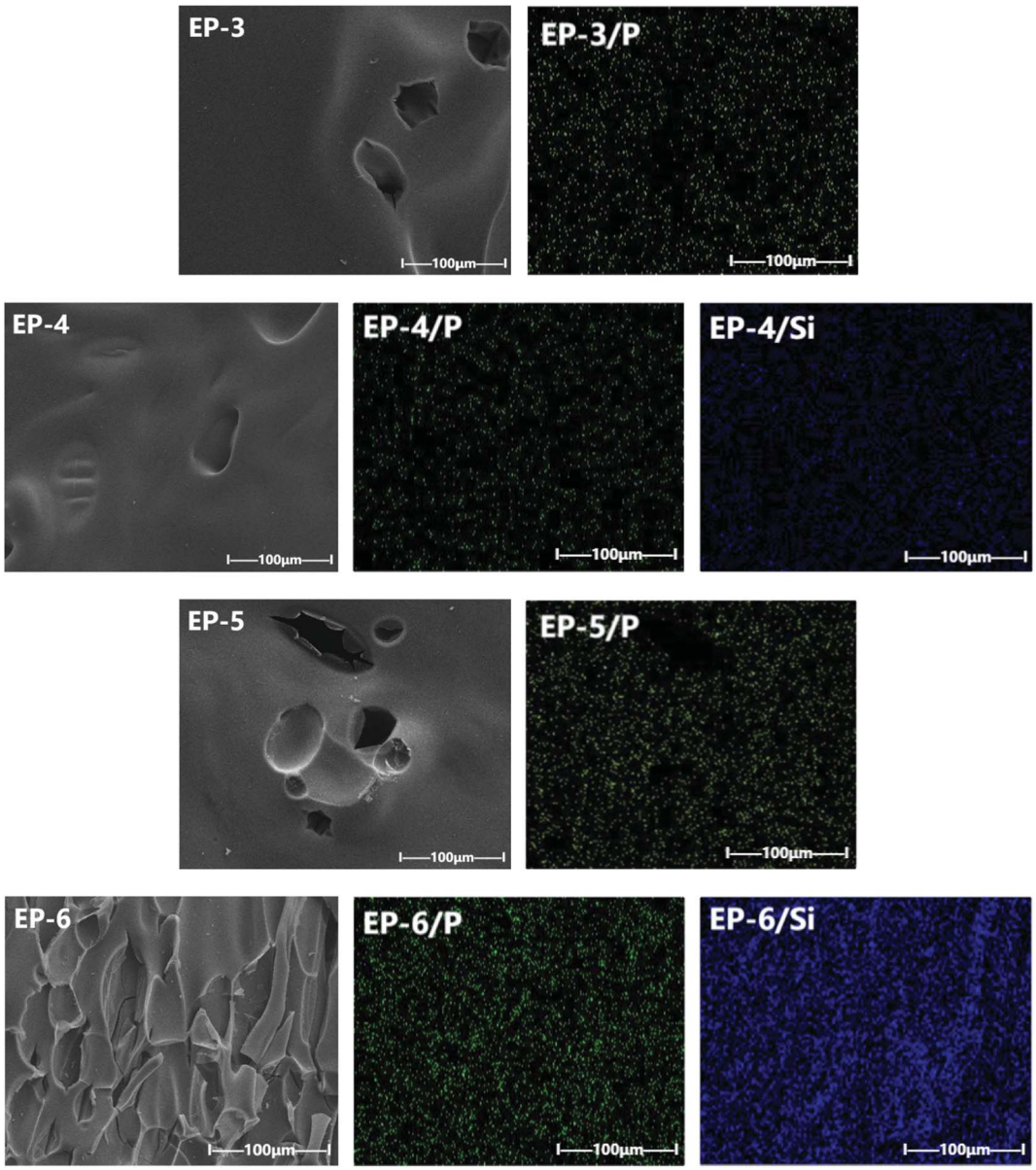

Fig. 8 EDX element mapping images of POSS/D-bp/DGEBA hybrid composites after cone calorimeter test (scale bar size: 100 μm).

cone calorimeter test. It can be observed from EP-1 and EP-3 that the broad stretching vibration of N–H and O–H bonds is around 3443 cm^{-1}, and it is attributed to the existence of the hydroxy and ammonium compounds in the condensed phase. In addition, the absorption peak at 1646 cm^{-1} is ascribed to the carbonized networks. A broad absorption of P–O–P bond discerned at around 1102 cm^{-1} suggests the presence of phosphorus-containing compounds in the char layer. Moreover, there are some discrepancies between the spectrum of EP-3 and EP-6, in which several new peaks are presented at 951 cm^{-1} (Si–O–phenyl) and at 798 and 466 cm^{-1} (Si–O). The above results further indicate that silicon-containing compounds, which derived from the degradation of G-POSS participate to construct a stable carbon layer with the phosphorus one in the condensed phase.

3.3.4 XPS analysis. In order to verify the FT-IR analysis, the elemental composition of collected exterior char residues is investigated by XPS analysis and the contents of C, N, O, P and Si elements are listed in Table 5. It is found that the content of C element in the char residue of EP-3 is higher than that of EP-1 and small quantity of P element is also detected, which clearly indicates the participation of phosphorus-containing compounds in the construction of char layer. Moreover, the content of P element in the char residues are higher than that before combustion. Si and O elements are discovered in EP-4 and the ratios increase in EP-6. The emergence of Si and O elements may come from the existence of abundant silica in the char residue after combustion, which is beneficial to enhance the stability of char layer. The XPS results reveal that G-POSS and D-bp have obviously synergistic flame retardation effect

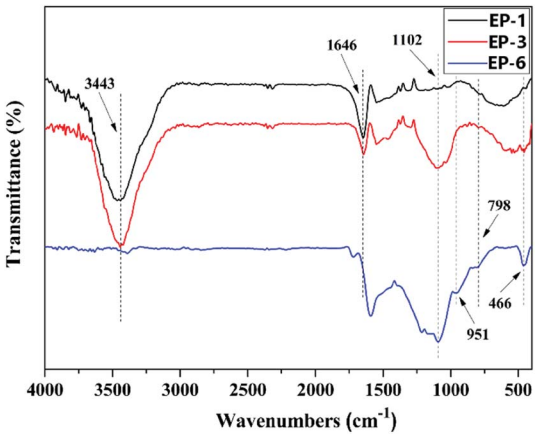

Fig. 9 FT-IR spectra of the char residues for the samples of EP-1, EP-3 and EP-6.

Table 5 XPS analysis of the char residues after the cone calorimeter test

Samples	C (wt%)	N (wt%)	O (wt%)	P (wt%)	Si (wt%)
EP-1	80.89	4.20	14.91	0	0
EP-2	82.56	2.78	9.94	0	4.72
EP-3	82.79	13.11	3.77	0.33	0
EP-4	78.18	4.08	13.97	0.31	3.46
EP-5	85.88	9.77	3.61	0.74	0
EP-6	53.49	2.38	25.67	1.47	16.99

in the condensed phase, which intuitively shown that the content of the corresponding elements in the char residues increase significantly.

3.4 Mechanical properties of POSS/D-bp/DGEBA hybrid composites

In addition, tensile and flexural strength tests are used to evaluate the mechanical properties of POSS/D-bp/DGEBA hybrid composites. Fig. 10 shows their tensile stress/strain curves and the corresponding tensile and flexural properties data are also listed in Table 6. Due to the phosphorus-containing groups would greatly reduce the crosslink density of cured epoxy resin, the tensile strength and the integral area of discharge based on the tensile stress/strain curve are obviously declined with the incorporation of D-bp. On the contrary, tensile strength and integral area of discharge have a considerable ameliorated with the introduction of G-POSS and tensile modulus has further enhanced. It is worth noting that EP-4 have a synergistic flame retardation effect between D-bp and G-POSS for the tensile properties, which is reflected in the tensile strength and the integral area of discharge are increased by 14.5% and 54.8% on the basis of EP-1, respectively. The similar tendency also can be found in flexural properties test with the flexural strength of EP-4 reaches the maximum value of 125.8 MPa, which is increased by 20.2 MPa compared with EP-1. Besides, the tensile and flexural modulus of POSS/D-bp/DGEBA hybrid composites are enhanced which depend on the collective effect of rigidity D-bp and G-POSS structure. The above results indicated that the rigid inorganic Si–O–Si core of G-POSS serves as highly functional anchors and the flexible organic branches plays a toughening effect on the DGEBA matrix, which effectively eliminate the influence of D-bp. On the whole, the mechanical properties of POSS/D-bp/DGEBA hybrid composites are elevated after the addition of G-POSS.

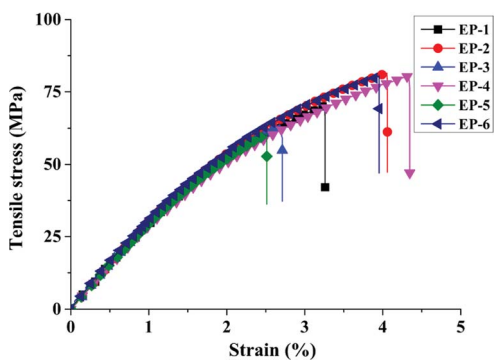

Fig. 10 Tensile stress/strain curves of POSS/D-bp/DGEBA hybrid composites.

3.5 DMA of POSS/D-bp/DGEBA hybrid composites

To further demonstrate the influence of curing behavior by D-bp and G-POSS, DMA is used to determine the crosslinking density of POSS/D-bp/DGEBA hybrid composites. Fig. 11 and 12 are exhibited the loss tangent (tan δ) and storage modulus curves of POSS/D-bp/DGEBA hybrid composites, respectively. Besides, the relation data of DMA are listed in Table 7 while T_g is obtained from the peak temperature of tan δ in Fig. 11. Compared with EP-1, T_g of EP-3 and EP-5 decline obviously following the introduction of D-bp alone, which is attributed to the phosphorus-containing group would reduce the crosslink densities of cured epoxy resins. In contrast, due to the introduction of G-POSS owns superior thermal stability, EP-2 shows an obviously increase in T_g and reaches up to 183.9 °C, which is increased by 19.4 °C than that of EP-1. The similar trend also can be observed from EP-4, which considerably increased by 16.2 °C compared with EP-1. In the condition of the same phosphorus content, POSS/D-bp/DGEBA hybrid composites exhibit a higher T_g than that only modified by D-bp. The above results reflect the significant reinforcement effect on T_g by G-POSS.

The variation of T_g is associated with crosslink density (ν_e). According to the literature, ν_e values can be calculated by the rubber elasticity theory[30,31] with the eqn (1):

$$\nu_e = E'/3RT \quad (1)$$

where E' is the storage modulus at T_g + 40 °C in the rubbery plateau, R is the ideal gas constant, T is the thermodynamic temperature at T_g + 40 °C.

The calculation results of ν_e according to the above formulation also listed in Table 7. Clearly, it is consistent with the tendency of tan δ that the calculation results of ν_e are transformed progressively to a higher value with the introduction of

Table 6 Mechanical properties results of POSS/D-bp/DGEBA hybrid composites

Samples	Tensile strength (MPa)	Tensile modulus (GPa)	Flexural strength (MPa)	Flexural modulus (GPa)
EP-1	70.3 ± 1.3	2.88 ± 0.08	105.6 ± 3.1	2.78 ± 0.13
EP-2	81.5 ± 4.0	3.60 ± 0.14	119.7 ± 2.6	2.79 ± 0.07
EP-3	63.7 ± 1.7	3.05 ± 0.11	99.8 ± 1.5	3.05 ± 0.05
EP-4	80.5 ± 1.2	3.71 ± 0.06	125.8 ± 2.5	3.19 ± 0.09
EP-5	60.5 ± 2.8	3.61 ± 0.18	94.7 ± 2.3	3.21 ± 0.11
EP-6	80.5 ± 1.0	4.07 ± 0.16	123.1 ± 1.8	3.31 ± 0.12

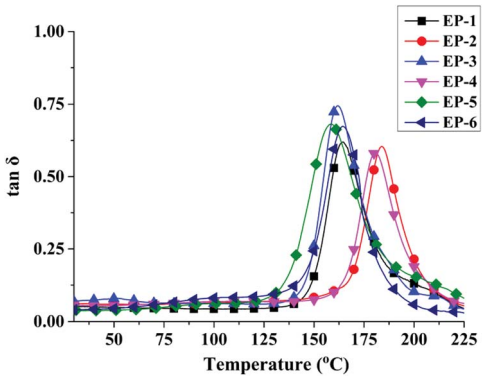

Fig. 11 tan δ curves of POSS/D-bp/DGEBA hybrid composites.

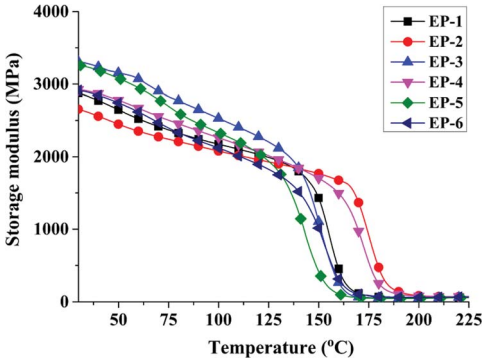

Fig. 12 Storage modulus curves of POSS/D-bp/DGEBA hybrid composites.

Table 7 DMA data of POSS/D-bp/DGEBA hybrid composites

Samples	T_g (°C)	tan δ	E' (MPa)	ν_e (10^3 mol m^{-3})
EP-1	164.5	0.62	60.8	5.11
EP-2	183.9	0.60	72.4	5.84
EP-3	161.8	0.74	53.4	4.51
EP-4	180.7	0.58	79.8	6.48
EP-5	158.5	0.67	48.8	4.15
EP-6	164.4	0.67	63.1	5.30

G-POSS. It is noteworthy that in the condition of same phosphorus content, ν_e of EP-4 reaches the maximum value of 6.48 × 10^3 mol m^{-3} which increased by 30.4% compared with EP-3. The reasonable explanation is that the reactive glycidyl group of rigid G-POSS participates in the crosslinking reaction of epoxy resin, which hinders the movement of the polymer chains and then significantly increases ν_e of hybrid composites. Besides, the storage modulus of EP-4 and EP-6 are higher than that of EP-1 at room temperature, illustrating the rigidity of POSS/D-bp/DGEBA hybrid composites are enhanced. The above results indicated that G-POSS acts as reactive reinforcement, which enhances the dynamic mechanical properties of POSS/D-bp/DGEBA hybrid composites effectively.

4. Conclusion

A series of high-performance hybrid epoxy composites were prepared *via* crosslinking reaction among flame retardant co-curing agent D-bp, reinforcement agent G-POSS and matrix DGEBA. Probably owing to the phosphorus–silicon synergistic flame retardation effect and nano-enhancement effect by incorporation of G-POSS that POSS/D-bp/DGEBA hybrid composites exhibit excellent comprehensive performance, in which the V-0 grade of UL-94 classification is achieved and P-HRR is significantly decreased from 939 kW m^{-2} to 371 kW m^{-2} when the phosphorus content is only 0.25 wt%. What's more, G-POSS can effectively compensate the decrease of thermal stability and mechanical properties influenced by D-bp. Compared with the neat sample, T_g is increased by 16.2 °C meanwhile the tensile and flexural strengths have obviously improved, which are increased by 12.7% and 16.1% respectively. Therefore, POSS/D-bp/DGEBA hybrid composites are expected to be used as high-performance composite materials in semiconductor encapsulation applications.

Conflicts of interest

There are no conflicts to declare.

Acknowledgements

This research was supported by Guangxi Natural Science Foundationunder Grant No. 2019GXNSFBA185020 and The Open Fund for Key Lab of Guangdong High Property and Functional Macromolecular Materials, China (20190019).

References

1 S. Levchik, A. Piotrowski, E. Weil and Q. Yao, *Polym. Degrad. Stab.*, 2005, **88**, 57–62.

2 F. L. Jin, X. Li and S. J. Park, *J. Ind. Eng. Chem.*, 2015, **29**, 1–11.
3 S. Q. Huo, P. A. Song, B. Yu, S. Y. Ran, V. S. Chevali, L. Liu, Z. P. Fang and H. Wang, *Prog. Polym. Sci.*, 2021, **114**, 101366.
4 H. Wang, S. Li, Z. M. Zhu, X. Z. Yin, L. X. Wang, Y. X. Weng and X. Y. Wang, *Polym. Degrad. Stab.*, 2021, **183**, 109426.
5 M. M. Velencoso, A. Battig, J. C. Markwart, B. Schartel and F. R. Wurm, *Angew. Chem., Int. Ed.*, 2018, **57**, 1–18.
6 P. Wang, L. Xia, R. K. Jian, Y. F. Ai, X. L. Zheng, G. L. Chen and J. S. Wang, *Polym. Degrad. Stab.*, 2018, **149**, 69–77.
7 P. Wang and Z. Cai, *Polym. Degrad. Stab.*, 2017, **137**, 138–150.
8 X. Lu, M. Yu, D. Wang, P. Xiu, C. Xu, A. F. Lee and X. Gu, *Mater. Today Chem.*, 2021, **22**, 100562.
9 S. Q. Huo, J. Wang, S. Yang, C. Li, X. L. Wang and H. P. Cai, *Polym. Degrad. Stab.*, 2019, **159**, 79–89.
10 X. Han, R. Chen, M. Yang, C. B. Sun, K. Wang and Y. S. Wang, *High Perform. Polym.*, 2022, **34**, 173–183.
11 W. Q. Xie, S. W. Huang, D. L. Tang, S. M. Liu and J. Q. Zhao, *RSC Adv.*, 2020, **10**, 8054.
12 A. Wirasaputra, X. H. Yao, Y. M. Zhu, S. M. Liu, Y. C. Yuan, J. Q. Zhao and Y. Fu, *Macromol. Mater. Eng.*, 2016, **301**, 982–991.
13 D. M. Min, H. Z. Cui, Y. L. Hai, P. X. Li, Z. J. Xing, C. Zhang and S. T. Li, *Compos. Sci. Technol.*, 2020, **199**, 108329.
14 Y. H. Zhang, L. Li, K. M. Nie and S. X. Zheng, *Mater. Chem. Phys.*, 2020, **240**, 122183.
15 J. L. Li, H. Y. Wang and S. C. Li, *High Perform. Polym.*, 2019, **31**, 1217–1225.
16 B. R. Zeng, R. R. Zhou, X. H. Zheng, J. Y. Ye, J. M. Chen, Y. T. Xu, C. H. Yuan and L. Z. Dai, *Polym. Adv. Technol.*, 2021, **32**, 2339–2351.
17 X. Han, X. H. Zhang, Y. Guo, X. Y. Liu, X. J. Zhao, H. Zhou, S. L. Zhang and T. Zhao, *Polymers*, 2021, **13**, 1363.
18 L. C. Liu, W. C. Zhang and R. J. Yang, *Polym. Adv. Technol.*, 2020, **31**, 2058–2074.
19 J. M. Luo, R. Li, H. W. Zou, Y. Chen and M. Liang, *High Perform. Polym.*, 2018, **31**, 800–809.
20 X. M. Ye, J. J. Li, W. C Zhang, R. J. Yang and J. R. Li, *Composites, Part B*, 2020, **191**, 107961.
21 Y. Q. Shi, B. Yu, Y. Y. Zheng, J. Guo, B. H. Chen, Z. M. Pan and Y. Hu, *Polym. Adv. Technol.*, 2018, **29**, 1242–1254.
22 C. Liu, T. Chen, C. Yuan, Y. Chang, G. Chen, B. Zeng, Y. Xu, W. Luo and L. Dai, *RSC Adv.*, 2017, **7**, 46139–46147.
23 W. C. Zhang, X. M. Li and R. J. Yang, *Polym. Degrad. Stab.*, 2012, **97**, 1314–1324.
24 W. C. Zhang, X. M. Li and R. J. Yang, *Polym. Degrad. Stab.*, 2011, **96**, 2167–2173.
25 W. C. Zhang, G. Camino and R. J. Yang, *Prog. Polym. Sci.*, 2017, **67**, 77–125.
26 C. Liu, T. Chen, C. H. Yuan, C. F. Song, Y. Chang, G. R. Chen, Y. T. Xu and L. Z. Dai, *J. Mater. Chem. A*, 2016, **4**, 3462–3470.
27 W. H. Xu, A. Wirasaputra, S. M. Liu, Y. C. Yuan and J. Q. Zhao, *Polym. Degrad. Stab.*, 2015, **122**, 44–51.
28 J. Wang, C. Ma, P. Wang, S. Qiu, W. Cai and Y. Hu, *Polym. Degrad. Stab.*, 2018, **149**, 119–128.
29 Y. Q. Shi, T. Fu, Y. J. Xu, D. F. Li, X. L. Wang and Y. Z. Wang, *Chem. Eng. J.*, 2018, **354**, 208–219.
30 P. H. Henna and R. C. Larock, *Macromol. Mater. Eng.*, 2007, **292**, 1201–1209.
31 B. Francia, S. Thomas, R. Sadhana, N. Thuaud, R. Ramaswamy, S. Jose and L. Rao, *J. Polym. Sci., Part B: Polym. Phys.*, 2007, **45**, 2481–2496.